PHYSICAL REVIEW B VOLUME 5, NUMBER 5 1 MARCH 1972

Dispersion and Damping of Soft Zone-Boundary Phonons in $KMnF_3$

K. Gesi,* J. D. Axe, and G. Shirane
Brookhaven National Laboratory, Upton, New York 11973

and

A. Linz
Center for Material Science and Engineering, Massachusetts Institute of Technology, Cambridge, Massachusetts 02139

(Received 9 August 1971)

Neutron inelastic-scattering experiments have been performed upon the cubic perovskite phase of $KMnF_3$. The anisotropy in the dispersion of the lowest-energy phonon branch around the R point [$\vec{q}_R = (\frac{1}{2}, \frac{1}{2}, \frac{1}{2})a^*$] has been determined. The phonon energies remain very low for $(\vec{q} - \vec{q}_R)$ along [100], which accounts for the anisotropic x-ray diffuse scattering seen in this material. The energy profiles of the soft modes at $(\frac{1}{2}\frac{1}{2}\frac{1}{2})(\Gamma_{25})$ and $(\frac{1}{2}\frac{1}{2}0)(M_3)$ are analyzed on the basis of a damped-harmonic-oscillator model taking into account the effect of the instrumental resolution. For the Γ_{25} mode, the temperature dependence of the characteristic frequency ω_0 is represented by a Curie-Weiss law $(\hbar\omega_0)^2 = C(T - T_0)$ with $C = 0.11 \pm 0.02$ meV^2 °K^{-1} and $T_0 = (186 \pm 2)$ °K. The damping parameter Γ increases as the temperature approaches T_0.

I. INTRODUCTION

Recently it has been shown that the structural phase transformations in several perovskite crystals result from an instability of the low-energy phonon branch at the Brillouin zone corner (R point) of the cubic structure. Neutron-inelastic-scattering experiments have provided the most direct evidence for the zone-boundary phonon condensation in $SrTiO_3$[1] (transition point $T_c = 105$ °K), $LaAlO_3$[2] ($T_c = 530$ °K), and $KMnF_3$[3-5] ($T_c = 186$ °K). The lower symmetry structures below T_c are distorted by the appearance of static displacements transforming according to the triply degenerate Γ_{25} representation of the group of the wave vector R, and involving only rotation of the oxygen (or fluorine in the case of $KMnF_3$) octahedra.[6]

The crystal structure of $KMnF_3$ below the 186 °K transition was reported to be orthorhombic by earlier x-ray work.[7] However, recent reexamination by Minkiewicz *et al.*[8] showed that it rather belongs to the tetragonal space group $I4/mcm$ (D_{4h}^{18}), the same symmetry as the low-temperature phase of $SrTiO_3$.[1] Therefore, the mechanism of the 186 °K phase transition in $KMnF_3$ is considered to be identical with that of the 105 °K phase transition in $SrTiO_3$. Only one of the three degenerate modes of Γ_{25} condenses at the transition point.[8] At 91.5 °K, $KMnF_3$ undergoes a second structural phase transition,[5] and the crystal transforms to a monoclinic structure.[7] This transformation is also known to involve the instability of a phonon of symmetry M_3 with $\vec{q}_M = (\frac{1}{2}\frac{1}{2}0)a^*$. The 186 °K transition is of the first order, but close to second order[5,9] with $(T_c - T_0) = 0.5$ °K. Slightly below the lower structural-transition temperature, at 88.0 °K, antiferromagnetic spin order is established.[5] Thus the problem of the phase stability in $KMnF_3$ is on the whole rather complicated. In the present paper, attention is concentrated exclusively on the cubic phase. Previous neutron-scattering work[3-5] gave a qualitative picture of the behavior of the soft phonons at R and M reciprocal-lattice points. The phonon energies of Γ_{25} and M_3 modes are low, about 3 meV even at room temperature. When the temperature is lowered, these modes soften further and become overdamped, i.e., the energy profile of the phonons peaks at $E = 0$.

The purpose of the present work is twofold: to provide quantitative description of the lowest-energy phonon dispersion surfaces around the R point, and to describe the evolution of the damping of the zone-boundary phonons quantitatively. The knowledge of the dispersion surfaces can provide important information for the analysis of the fluctuations, thermodynamic properties, and other characteristics of the $KMnF_3$ transformation. The study of the soft-mode line shape has revealed an unexpected singularity in the damping near the transformation temperature. In Sec. III the results of the dispersion-surface measurements will be described. A phenomenological expression of the lowest-energy phonon branches is shown to represent the observed anisotropy very well. The phonon energy profiles are analyzed in Sec. IV on the basis of a damped-harmonic-oscillator model taking into account instrumental resolution, and the temperature dependence of the damping parameter is obtained. Finally, Sec. V describes the intensity distribution for x-ray diffuse scattering around the R point, which is calculated from the anisotropic phonon dispersion. The results are compared with previous x-

ray results.

II. EXPERIMENTAL

The single crystals of $KMnF_3$ were grown from a melt containing a few percent excess of KF as the solvent by means of a modified Czochralski method in a purified helium atmosphere. Two crystals were used in the present study, one nearly perfect (volume 10 cm^3; mosaic spread 4′ of arc), the other smaller and less perfect (1 cm^3; 20′ mosaic). No important differences between the two crystals were observed.

Neutron inelastic measurements were performed on a triple-axis spectrometer at the Brookhaven high-flux beam reactor in the constant-Q mode with the incident neutron energy of 45 meV. Germanium (311) and pyrolytic graphite (004) reflections were used as the monochromator and analyzer, respectively. Some supplemental higher-resolution measurements were made at 14 meV at temperatures near T_c. For the over-all survey experiments, standard (hhl) and $(hk0)$ zones were used. The strongly anisotropic scattering along $\langle 100\rangle$ directions $(R \rightarrow M)$ is not observed in these zones, which caused us to investigate the unconventional $(h, k, 3k)$ scattering plane for the line-profile analysis (see Fig. 1). The specimen temperature was controlled to within ± 1 °K for the high-temperature experiments, and to within ± 0.1 °K for the low-temperature experiments.

III. PHONON DISPERSION

The dispersion relations of low-energy phonon branches are indicated in Fig. 2 for the three high-symmetry directions $[\zeta 00]$, $[\zeta\zeta 0]$, and $[\zeta\zeta\zeta]$ at room temperature. The lowest-energy transverse branch Σ_3 and Λ_3 terminate at the zone boundary at a very low energy of about 3 meV even at room temperature.[10]

The lowest-energy phonon dispersion surfaces around the R point can be expressed by a small-q expansion given in the Appendix. The parameters $\lambda_1, \lambda_2, \lambda_3$ in the dynamical matrix $\underline{C}^T(\vec{\eta})$ can be deduced from the observed curvature of the branches along high-symmetry directions. Along the [100] direction, the eigenvalues of $\underline{C}^T(\vec{\eta})$ are

$$\hbar^2\omega_1^2(T_2) = \hbar^2\omega_0^2 + \lambda_1(\vec{q} - \vec{q}_R)^2 \quad \text{(nondegenerate)}$$

and

$$\hbar^2\omega_1^2(T_5) = \hbar^2\omega_0^2 + \lambda_2(\vec{q} - \vec{q}_R)^2 \quad \text{(twofold degenerate)}.$$

The observed dispersion at room temperature is shown in Fig. 3. The nondegenerate (T_2) branch is nearly flat from R to M, while the doubly degenerate T_5 branch has a pronounced curvature. Then, we get $\lambda_1 \approx 0$, $\lambda_2 = 710$ meV^2 Å^2. λ_3 can be determined to be 100 meV^2 Å^2 from the observed doubly degenerate Λ_3 branch along the [111] direction which corresponds to the eigenvalue of

$$\hbar^2\omega_1^2(\Lambda_3) = \hbar^2\omega_0^2 + \tfrac{1}{3}(\lambda_1 + 2\lambda_2 - \lambda_3)(\vec{q} - \vec{q}_R)^2.$$

By using $\lambda_1, \lambda_2, \lambda_3$ determined in this way the phonon dispersion in an arbitrary direction of $\vec{\eta} = \vec{q} - \vec{q}_R$ can be calculated as the eigenvalues of $\underline{C}^T(\vec{\eta})$.

Figure 4 shows the anisotropic behavior of the phonon branch curvature in the $(1\bar{1}0)$ plane. Along the [001] direction, we have a very flat nondegenerate branch $[\Lambda \equiv \frac{1}{2}\partial^2(\omega_1^2)/\partial\eta^2 \approx 0]$ and a doubly degenerate (T_5) branch. As the direction of $\vec{\eta}$ goes away from [001], the latter degeneracy is removed, until for the [111] direction the two lower branches coalesce into doubly degenerate Λ_3 branch. Finally, along the [110] direction we have three nondegenerate branches, of which only the lowest S_1 branch has nonvanishing structure factor in the (hhl) zone. The calculated Λ for the S_1 branch, 305 meV^2 Å^2, represents the observed points very well, as shown in Fig. 3, and serves as an independent check on the validity of the procedure.

IV. DAMPING

At and above room temperature, the characteristic phonon frequency ω_0 for the Γ_{25} mode can be accurately determined from line-profile analysis, and ω_0^2 obeys a Curie-Weiss law:

$$\hbar^2\omega_0^2 = A(T - T_0) \qquad (1)$$

as shown in Fig. 5. In the lower temperature region, the effect of overdamping prevents accurate determination of ω_0 and Γ independently. However, assuming the validitiy of Eq. (1), the integrated intensity I is proportional to T/ω_0^2,[4,6] and the relative temperature dependence of ω_0^2 can be obtained by plotting T/I against T. This plot is indicated by the solid circles in Fig. 5, showing again a Curie-

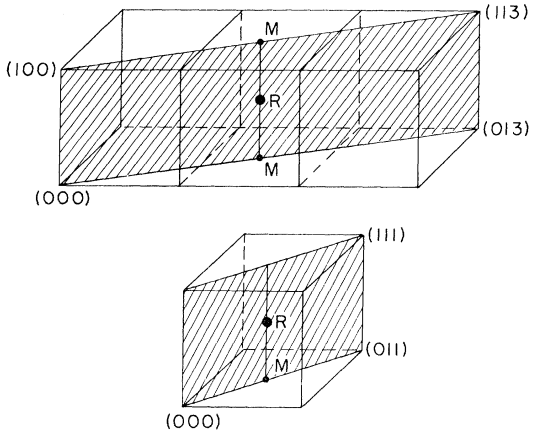

FIG. 1. Diagram showing the two scattering planes in reciprocal space used in this study. Selection rules forbid scattering from the soft branch extending from $R \rightarrow M$ in the conventional (h, k, k) zone (below).

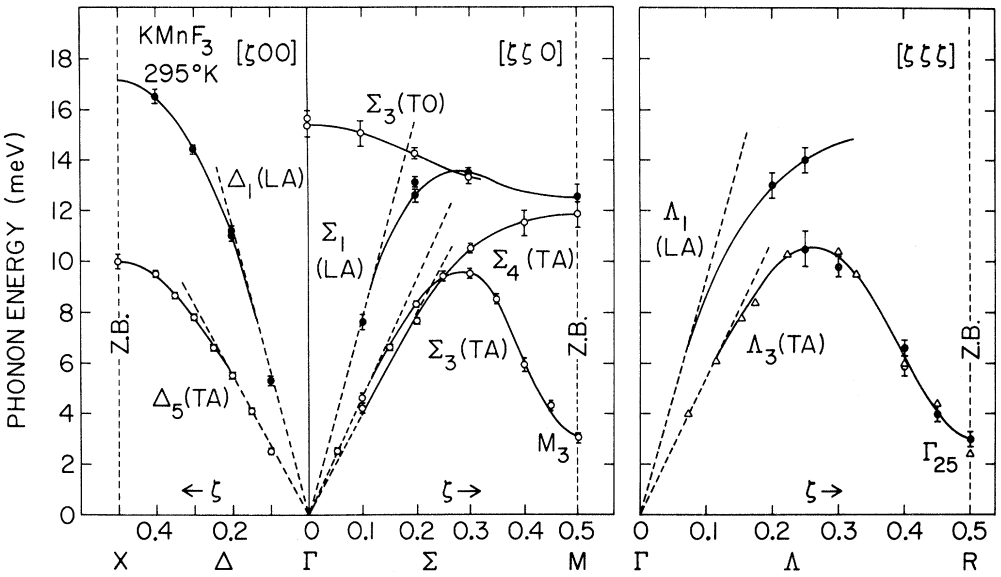

FIG. 2. Low-energy phonon dispersion curves along the three high-symmetry directions of $KMnF_3$ measured at 295 °K. The open and closed circles, respectively, indicate the data taken with a transverse and a longitudinal spectrometer setting. The triangles show the results of Minkiewicz and Shirane (Ref. 3) at 280 °K. The dotted lines indicate the sound velocity calculated by the elastic constants.

Weiss behavior in the overdamped region. Thus it is very plausible to conclude that the Curie-Weiss law [Eq. (1)] holds over the whole temperature studied. The constant A is determined to be 0.11 ± 0.02 meV^2 °K and $T_0 = (186 \pm 2)$ °K, in good agreement with the value of $186.0(\pm 0.2)$ °K given in Ref. 6.

The phonon-energy profiles of the Γ_{25} and M_3 modes are shown in Figs. 6 and 7, respectively. In this experiment, the contribution from the magnetic diffuse scattering and from the $\frac{1}{2}\lambda$ contamination of the incident beam to the line profile around $\omega \approx 0$ is estimated to be less than 5% of the phonon scattering. At room temperature and above, the phonon profile has a well-defined peak, but the linewidth is appreciably larger than the instrumental resolution width even at the highest temperature studied. At temperatures lower than about 240 °K,

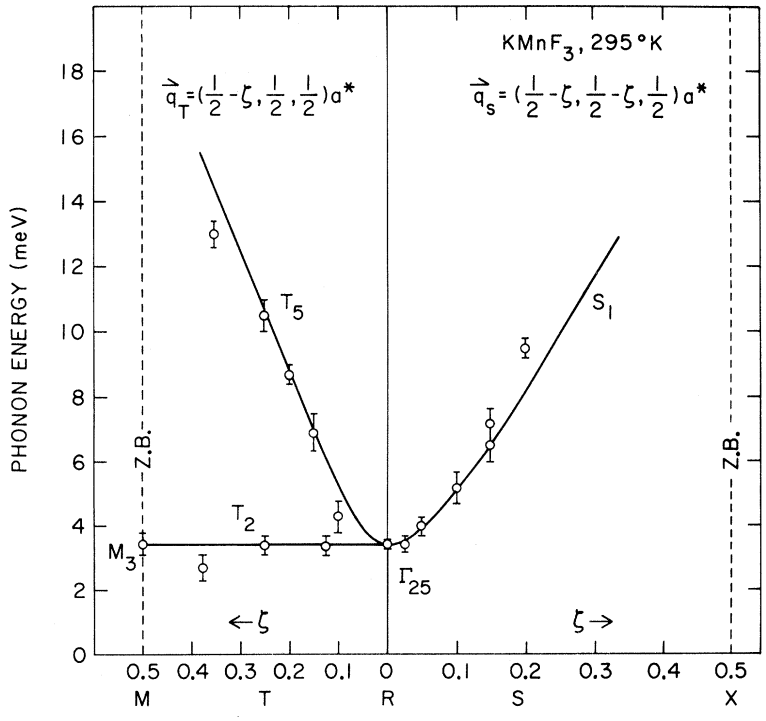

FIG. 3. Phonon dispersions in the vicinity of the R point in $KMnF_3$ at 295 °K. The solid curves in the figure show the calculated dispersion.

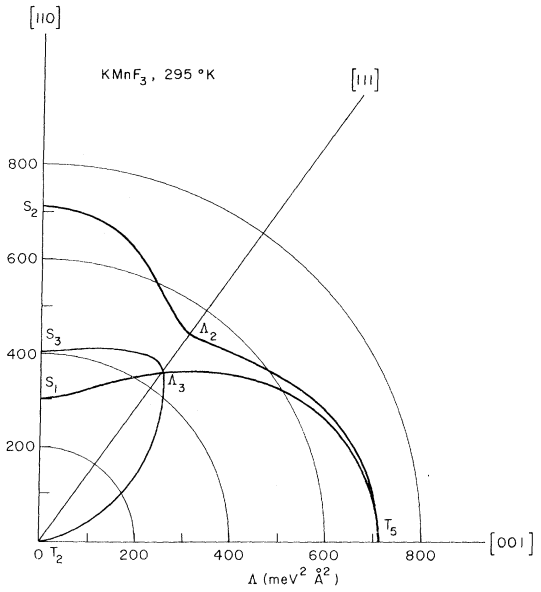

FIG. 4. Polar representation of the calculated angular dependence of the curvature Λ of the dispersion surfaces for the lowest-energy phonons around the R point in $KMnF_3$.

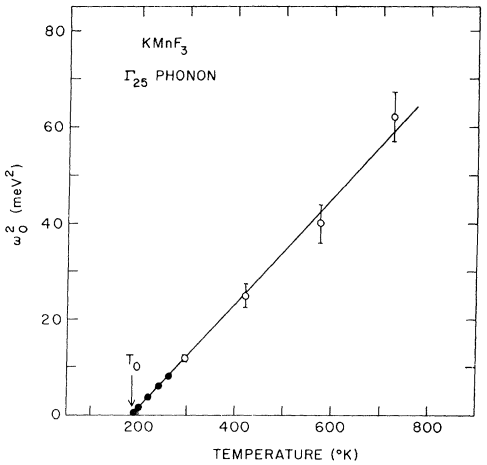

FIG. 5. Temperature dependence of $\hbar^2\omega_0^2$ for Γ_{25} mode of $KMnF_3$. The open circles represent the results of line-profile analysis, and the closed circles show T/I which are normalized so as to fit the higher-temperature data.

the phonon line shape becomes overdamped, and the profile has its maximum at $\omega = 0$.

The spectral-profile analysis was performed as follows. The cross section of the scattered neutron group is expressed by[1,3]

$$\frac{d^2\sigma}{d\Omega\, d\omega} = \frac{1}{\pi}\frac{k_F}{k_I}\,|F_{\text{in}}(\vec{Q})|^2[n(\omega,T)+1] \times \frac{\Gamma\omega}{[\omega_1^2(\vec{q},T)-\omega^2]^2+(\Gamma/\hbar)^2\omega^2}, \quad (2)$$

where $\hbar\vec{Q} = \hbar(\vec{k}_I - \vec{k}_F)$ and $\hbar\omega$ are the momentum and energy transfer in the scattering process, $n(\omega,T) = (e^{\beta\hbar\omega}-1)^{-1}$ is the phonon occupation number, $F_{\text{in}}(\vec{Q})$ is the inelastic structure factor, $\omega_1(\vec{q},T)$ is a temperature-dependent quasiharmonic mode frequency, and $\Gamma(\omega,T)$ is the damping parameter. Γ is an even function of ω, and, in the low-frequency approximation, it can be taken as a constant. The effect of the instrumental resolution is taken into account by making the convolution of Eq. (2) with the resolution function.[11]

In this analysis the "exact" dispersion relation for $\omega_1^2(\vec{q},T)$ given by $\underline{C}^T(\eta)$ was replaced by a single

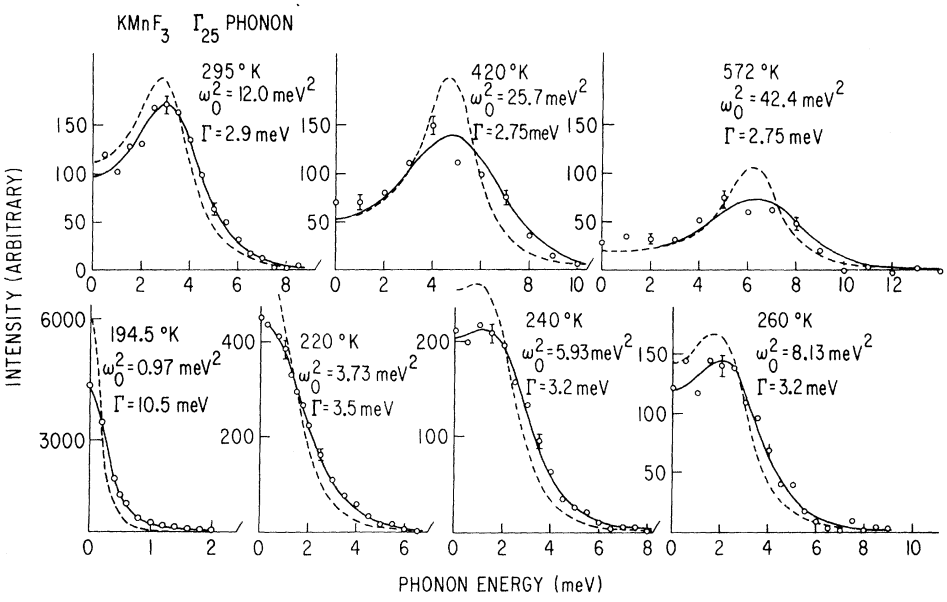

FIG. 6. Energy profiles of the Γ_{25} mode phonons of $KMnF_3$ at various temperatures. The circles are measured values; the dotted line the best-fitting cross section which is broadened by instrumental corrections to give the solid line. The data at the lowest temperature were taken with much higher resolution (note scale change).

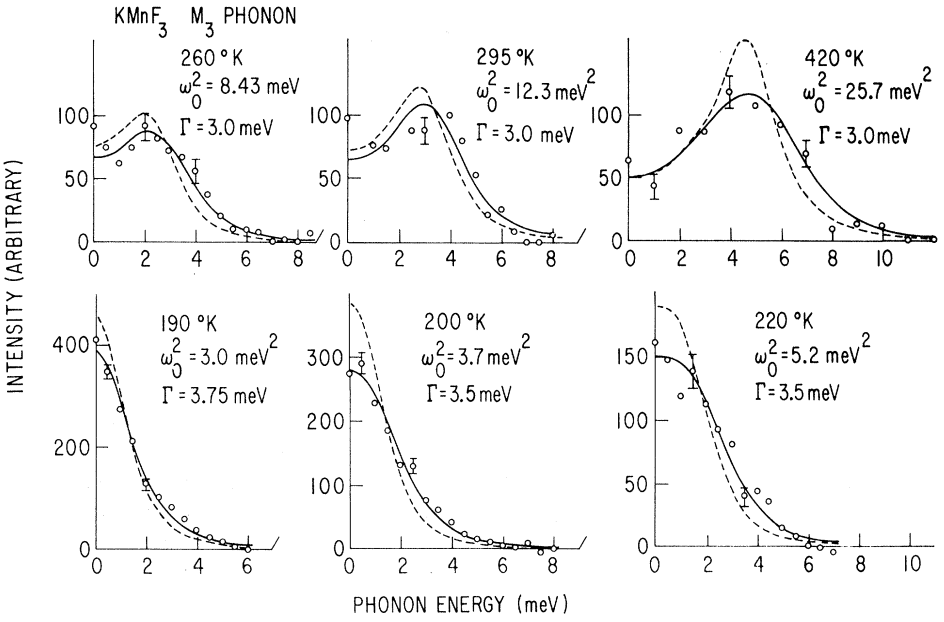

FIG. 7. Energy profiles of the M_3 mode phonons of $KMnF_3$ at various temperatures. The circles are measured values; the dotted line the best-fitting cross section which is broadened by instrumental corrections to give the solid line.

anisotropic branch chosen empirically to fit the observations in the scattering plane $(h, k, 3k)$ chosen. This procedure grossly oversimplifies the dispersion out of the scattering plane, but trial computations established that the relative line profile was not seriously affected by the assumed out-of-plane dispersion.

For the Γ_{25} mode, using the Curie-Weiss values for $\omega_0(T)$ discussed above, the damping parameter Γ is determined at each temperature so that the calculated line profile yields the best fit to the experimental results. The calculated line profiles are indicated by solid curves in Fig. 6. The intrinsic line profiles which we infer might be observed with zero instrumental resolution are also shown by the dotted curves. The effect of the finite resolution on the observed line profile becomes very serious only in the vicinity of the transition point, where the intrinsic linewidth is very narrow due to the strong overdamping. The temperature dependence of the damping parameter Γ for the Γ_{25} mode is shown in the upper part of Fig. 8.

For the M_3 mode, the temperature dependence of ω_0^2 estimated from the T/I-vs-T diagram shows a deviation from the Curie-Weiss law for Γ_{25} in the temperature range below about 240 °K, and ω_0^2 remains at a finite value at $T_0 = 186$ °K. Figure 9 shows the temperature dependence of ω_0^2 for the M_3 mode obtained from T/I normalized so as to fit the high-temperature phonon peak energy. The line profiles for the M_3 mode calculated by using the ω_0^2 shown in Fig. 9 are indicated by the solid curves in Fig. 7. Here the corresponding *intrinsic* line profiles are shown by the dotted curves. As shown in the lower part of Fig. 6, Γ also shows a slight increase with decreasing temperature for the M_3 mode, but has no singular behavior near T_0.

V. DISCUSSION AND CONCLUSION

Two x-ray studies of the diffuse scattering accompanying the 186 °K transformation in $KMnF_3$ have appeared recently.[8,12] Comès *et al.*[12] ob-

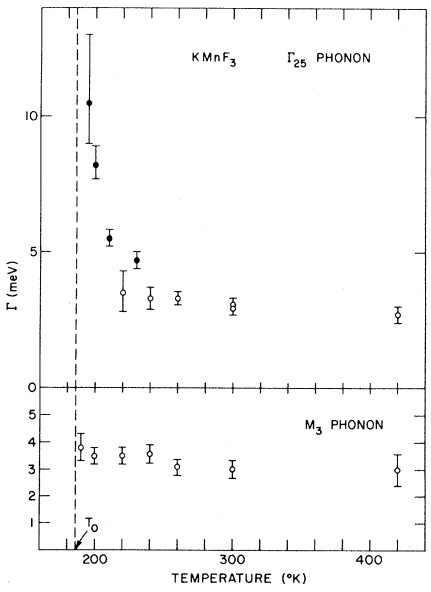

FIG. 8. Temperature dependence of the damping parameter Γ for the Γ_{25} mode (above) and the M_3 mode (below) phonons of $KMnF_3$. The open points were measured with 45-meV incident neutrons. The closed points represent higher-resolution measurements with 14-meV neutrons.

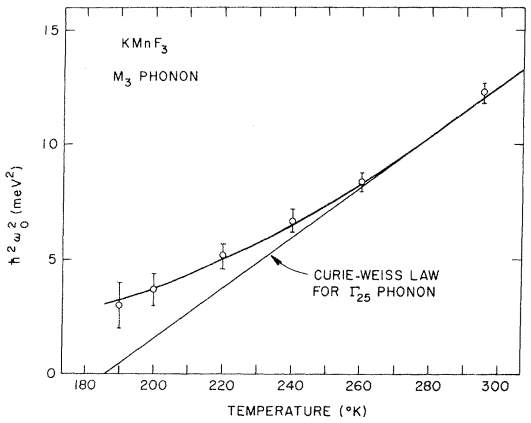

FIG. 9. Temperature dependence of ω_0^2 for M_3 mode of $KMnF_3$ estimated from T/I.

served rodlike diffuse streak along the ⟨100⟩ directions in the cubic phase. They discussed their results in terms of rotations of fluorine octahedra which are highly correlated within (100) layers but which are nearly incoherent from one layer to the next. We wish to point out that this is just the instantaneous picture which emerges for the rotations associated with the anisotropic phonon branches which we have discussed. If we denote the rotation of the fluorines of the lth unit cell about the α axis by $\phi_\alpha(l)$, then the instantaneous correlation of rotational fluctuations is

$$\langle \phi_\alpha(l)\phi_\beta(0)\rangle \propto \sum_{j\vec{q}} \left(\frac{e_\alpha(j\vec{q})e_\beta(j\vec{q})}{\omega_1^2(j\vec{q})}\right) e^{i\vec{q}\cdot\vec{R}_l}. \tag{3}$$

If the phonon dispersion is of the isotropic form $\omega_1^2(j\vec{q}) = \omega_0^2 + \Lambda|\vec{q}|^2$, the correlation is of the familiar Ornstein-Zernike type

$$\langle \phi_\alpha(l)\phi_\beta(0)\rangle \approx \delta_{\alpha\beta} e^{-\kappa R(l)}/R(l),$$

with $\kappa^2 = \omega_0^2/\Lambda$. In the present case, however, the sum over modes is heavily weighted by the soft branch with $\vec{q} - \vec{q}_R$ along [100] because of the inverse frequency factor, but this produces an additive effect upon $\langle \phi_\alpha(l)\phi_\beta(0)\rangle$ only if $\vec{q}\cdot\vec{R}(l) \approx 0$, i.e., if $\vec{R}(l)$ is in a {100} plane. Thus, at least qualitatively, the strongly anisotropic phonon dispersion necessarily leads to instantaneous, but *dynamical*, correlations of the type described by Comès *et al.*

We can put the discussion on a quantitative basis as follows. The x-ray diffuse scattering at a reciprocal-lattice vector $\vec{Q} = \vec{G} + \vec{q}_R + \vec{\eta}$ in the vicinity of an R point in the extended reciprocal lattice is given by

$$I(\vec{Q}) \propto \sum_{j=1}^{3} |F_j(\vec{Q})|^2 \frac{T}{\omega_1^2(j\vec{\eta})}, \tag{4}$$

where $\hbar\omega_1(j\vec{\eta})$ and $F_j(\vec{Q})$ are energy and inelastic structure factors of the jth mode, respectively. Equation (6) can readily be evaluated with the eigenvalues and eigenvectors of the dynamical matrix $\underline{C}(\vec{\eta})$ (Appendix). Figure 10(b) shows the calculated diffuse intensity scattered in a (100) plane about $\vec{Q} = \frac{1}{2}(33\bar{1})a^*$ at $T = T_0 + 0.9$ °K [corresponding to $(\hbar\omega_0)^2 = 0.1$ meV^2, about 0.6 °K above the transition point]. The rodlike streaks observed experimentally are clearly in evidence.

Minkiewicz *et al.*[8] made a more quantitative study of the distribution of the diffuse scattering near T_0 in a $(1\bar{1}0)$ scattering plane. Figure 10(a) shows the calculated intensity distribution for their scattering geometry. The most striking result is that the marked elongation of the distribution along the [001] direction just described is not present but is in fact reversed. The reason for this is that the structure factor for the *soft* (T_2) branch vanishes in this scattering plane, so that only scattering from the higher-lying (T_1) modes is observed. The calculated full width at half-maximum (FWHM), 0.024 Å^{-1}, along the [001] direction is in nearly perfect agreement with observation (0.025 Å^{-1}). Along the [110] direction, the calculated FWHM (0.037 Å^{-1}) is only half of the observed value. It appears that the discrepancy may be largely instrumental. Although the soft T_2 branch in the scattering plane (i.e., along [001]) cannot be observed, the similar modes along [100] and [010] do give strong scattering out of the chosen scattering plane. The finite vertical resolution (much coarser than the in-plane collimation[8]) samples this out of plane scattering, particularly during a scan along the [110] direction, and elongates the distribution. We have tried to indicate the source and extent of this effect in Fig. 10. Thus it appears that the pronounced and seemingly contradictory anisotropy in diffuse x-ray scattering[8,12] can be reconciled and arises from the soft phonon branches studied here.

There is a very simple qualitative explanation for the extremely anisotropic nature of the dispersion around R. Consider the rotation of a single octahedron of F ions about, say, the z axis. Since the four ions in the x-y plane which actually rotate are shared with neighboring octahedra, a highly correlated "cog-wheel" collective mode is favored. Because the sense of rotation changes from one cell to the next, the components of the favored wave vector in the x-y plane are $q_x = q_y = \pi/a$. There is, however, no similar short-range correlating force between adjacent *planes*, since the shared interplanar ions are stationary. Thus adjacent planes rotating with any phase between $\vec{q}_M = (\frac{1}{2}\,\frac{1}{2}0)$ and $\vec{q}_R = (\frac{1}{2}\,\frac{1}{2}\,\frac{1}{2})$ are nearly equally favorable energetically because all retain the perfect planar correlations.

Buyers *et al.*[4] analyzed the line profiles of the phonon group of Γ_{25} mode for pure and Co-doped

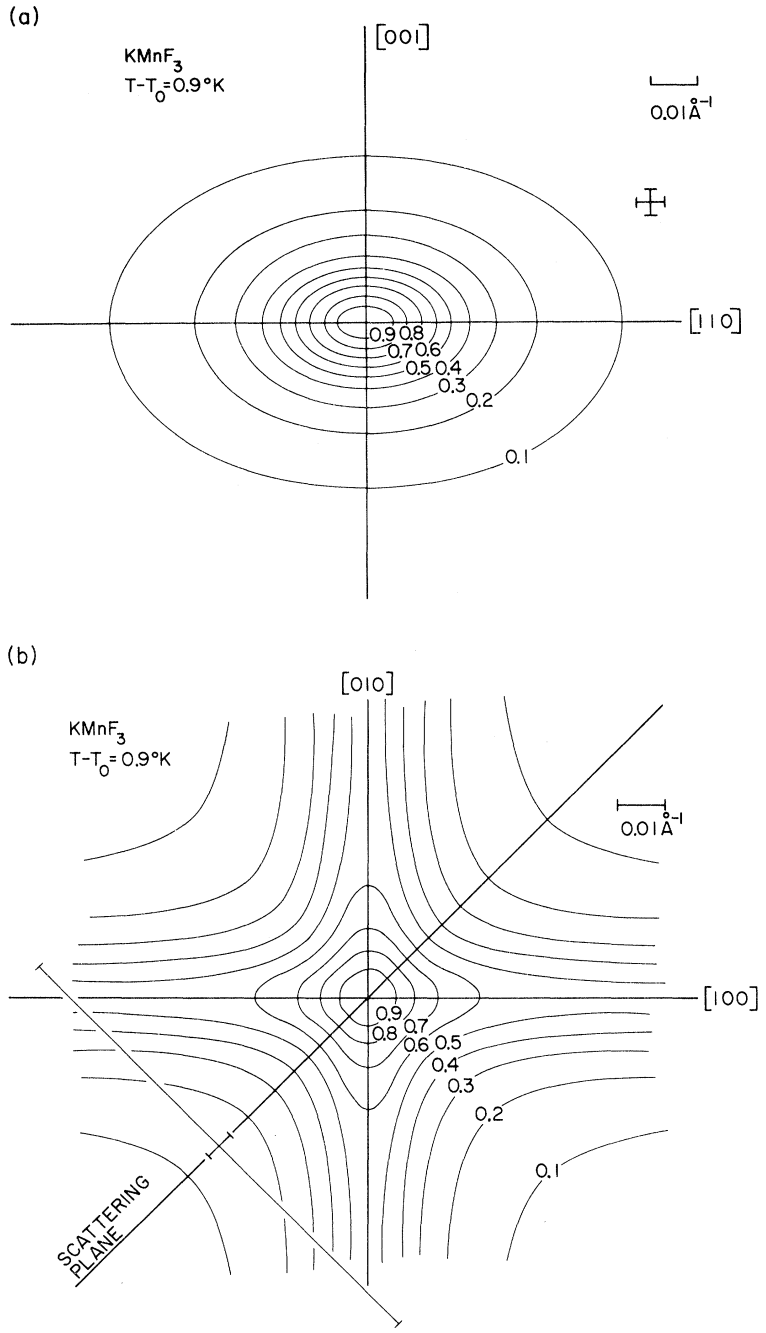

FIG. 10. Intensity contours for x-ray diffuse scattering of $KMnF_3$ around $\frac{1}{2}(33\bar{1})a^*$ at $T = T_0 + 0.9\,°K$: (a) in the $(1\bar{1}0)$ scattering plane; (b) in the (001) perpendicular to the scattering plane. The instrumental resolution of the x-ray experiment by Minkiewicz *et al.* is indicated by the cross marks. The vertical resolution represents 0.7° FWHM for Mo Kα radiation.

$KMnF_3$ crystals. For $KMnF_3$ they assumed a Curie-Weiss behavior for ω_0^2 and found $A = 0.130$ (± 0.004) meV^2 °K^{-1} and $T_c = 185.4 (\pm 0.3)$ °K, in reasonable agreement with the present values. They also found that a damping constant that was either temperature independent or weakly temperature dependent (proportional to T) was insufficient to explain their observed line shapes. Our more exact fitting procedure establishes that the damped oscillator response is adequate to understand existing data on $KMnF_3$ if a temperature dependent Γ is allowed. Burns and Scott[13] have reported similar behavior in $PbTiO_3$ in the ordered (polar) phase. Tani[14] predicted $\Gamma \sim (T - T_0)^{-1}$ for a one-dimensional model, but Pytte[15] pointed out that Γ is expected to show no singular behavior near T_0 for an isotropic three-dimensional model in lowest order. Clearly, the whole matter deserves further study.

Note added in proof. A recent reexamination of the overdamped soft-mode scattering just above the

transformation temperature with very high resolution has been made [S. M. Shapiro, J. D. Axe, G. Shirane, and T. Riste (unpublished)]. We find additional structure within what we have regarded here as a smooth single peak. It is now therefore clear that at least some of the unexpected behavior of the soft-mode damping must be attributed to a frequency dependent $\Gamma(\omega)$ rather than to a frequency independent $\Gamma(T)$.

An ESR study by Müller and Berlinger[16] found the temperature dependence of rotational displacement parameter to be described by $\sim(T_0 - T)^{0.33}$ for $SrTiO_3$ and $LaAlO_3$ in the temperature region immediately below the transition point. The critical exponent is considerably smaller than 0.5, which is predicted in the molecular field approximation. This result for the order parameter suggests that ω_0^2 might also deviate from the molecular field Curie-Weiss behavior in the vicinity of T_0. As shown in Fig. 5, no evidence for a strong deviation from the molecular field result for ω_0^2 is found in the present experiments. Of course, it is possible that such behavior is limited to a narrow critical-temperature region above T_0 which is physically inaccessible due to the first-order nature of the transformation.

ACKNOWLEDGMENTS

The authors are grateful to J. Skalyo, Jr. for making the computer program and for helpful discussions. They would like to thank W. Cochran, D. E. Cox, and V. J. Minkiewicz for many interesting discussions.

APPENDIX

We wish to put the dispersion of the phonon branches about the R point on a quantitative basis without resorting to a discussion of the complete lattice dynamics, which is formidable for a lattice of this complexity. This can be done by a generalization of the long-wavelength expansion used by Born and Huang[17] to discuss the macroscopic elastic behavior of a crystalline solid.

In the harmonic approximation the phonon frequencies as a function of wave vector $\vec{q}$ are the eigensolutions of the dynamical matrix $\underline{C}(\vec{q})$:

$$\underline{C}(\vec{q})\vec{e}(j\vec{q}) = \omega_j^2(j\vec{q})\vec{e}(j\vec{q}).$$

Since $\underline{C}(\vec{q})$ is a $3n \times 3n$ (15×15) matrix, there are $j = 1, 3n$ solutions for each value of $\vec{q}$. Suppose the three degenerate lowest eignestates of $\underline{C}(\vec{q}_R)$ are designated as $\vec{e}_x^0$, $\vec{e}_y^0$, $\vec{e}_z^0$. They are determined by symmetry considerations alone,[18] and can be chosen as rotations of F octahedra about the x, y, and z axes, respectively. We can form a truncated 3×3 dynamical matrix $\underline{C}^T(\vec{q})$ by the transformation

$$\underline{C}^T(\vec{q}) = \underline{U}^{-1}\underline{C}(\vec{q})\,\underline{U},$$

where $\underline{U}$ is the 3×15 matrix $(\vec{e}_x^0, \vec{e}_y^0, \vec{e}_z^0)$. By construction, at $\vec{q} = \vec{q}_R$, $\underline{C}^T(\vec{q})$ has the proper eigenvalues for the soft branch $\omega_1^2(j\vec{q}_R) \equiv \omega_0^2 (j = 1, 3)$. Consideration of the terms omitted from the full matrix $\underline{C}(\vec{q})$ shows that for small values of $\vec{\eta} \equiv \vec{q} - \vec{q}_R$, the eigenvalues of $\underline{C}^T(\vec{\eta})$ are in error by amounts of order $ca^4\eta^4$, where c is the magnitude of a typical element of $\underline{C}(\vec{q})$ and a is the unit cell dimension. Thus we may, exactly to terms of order η^2, determine the $\vec{q}$ dependence of the soft modes near $\vec{q}_R$ by expanding $\underline{C}^T(\vec{\eta})$ to η^2, obtaining

$$\underline{C}^T(\vec{\eta}) = \begin{bmatrix} \omega_0^2 + \lambda_1\eta_x^2 + \lambda_2(\eta_y^2 + \eta_z^2) & \lambda_3\eta_x\eta_y & \lambda_3\eta_x\eta_z \\ & \omega_0^2 + \lambda_1\eta_y^2 + \lambda_2(\eta_x^2 + \eta_z^2) & \lambda_3\eta_y\eta_z \\ \text{c.c.} & & \omega_0^2 + \lambda_1\eta_z^2 + \lambda_2(\eta_x^2 + \eta_y^2) \end{bmatrix}.$$

The form of $\underline{C}^T(\vec{\eta})$ is determined by the nature of the symmetry operations at $\vec{q} = \vec{q}_R$. Since the point symmetry is in fact O_h, if ω_0^2 is set to zero $\underline{C}^T(\vec{\eta})$ is identical to that matrix which determines the long-wavelength elastic modes in cubic crystals. [The proper correspondence is $\lambda_1 = C_{11}$, $\lambda_2 = C_{44}$, and $\lambda_3 = (C_{12} + C_{44})$.] The basis vectors, rather than being Cartesian displacements, are the rotations $\vec{e}_x^0$, $\vec{e}_y^0$, $\vec{e}_z^0$ and the eigenvectors are calculated accordingly. Once the eigenvectors $\vec{e}(j\vec{\eta})$ are known one can calculate the inelastic structure factor of the $j\eta$ mode:

$$F_j(\vec{Q}) = \sum_\kappa \vec{Q}\cdot\vec{e}_\kappa(j\vec{\eta})\, b_\kappa e^{i(\vec{G}\cdot\vec{r}_\kappa)}.$$

†Work performed under the auspices of the U. S. Atomic Energy Commission and Advanced Research Project Agency.

*Present address: Japan Atomic Energy Research Institute, Tokai-mura, Ibaraki-ken, Japan.

[1] G. Shirane and Y. Yamada, Phys. Rev. 177, 858 (1969).

[2] J. D. Axe, G. Shirane, and K. A. Müller, Phys. Rev. 183, 820 (1969).

[3] V. J. Minkiewicz and G. Shirane, J. Phys. Soc. Japan

26, 674 (1969).
[4]W. J. L. Buyers, R. A. Cowley, and G. L. Paul, J. Phys. Soc. Japan Suppl. 28, 242 (1970).
[5]G. Shirane, V. J. Minkiewicz, and A. Linz, Solid State Commun. 8, 1941 (1970).
[6]W. Cochran and A. Zia, Phys. Status Solidi 25, 273 (1968).
[7]O. Beckman and K. Knox, Phys. Rev. 121, 376 (1961).
[8]V. J. Minkiewicz, Y. Fujii, and Y. Yamada, J. Phys. Soc. Japan 28, 443 (1970).
[9]M. Furukawa, Y. Fujimori, and K. Hirakawa, J. Phys. Soc. Japan 29, 1528 (1970).
[10]In the following, we use the group-theoretical notation introduced in Ref. 18.
[11]M. J. Cooper and R. Nathans, Acta Cryst. 23, 357 (1967).
[12]R. Comès, F. Denoyer, L. Deschamps, and M. Lambert, Phys. Letters 34A, 65 (1971).
[13]G. Burns and B. A. Scott, Phys. Rev. Letters 25, 167 (1970).
[14]K. Tani, Phys. Letters 25A, 400 (1967).
[15]E. Pytte, Phys. Rev. B 1, 924 (1970).
[16]K. A. Müller and W. Berlinger (unpublished).
[17]M. Born and K. Huang, *Dynamical Theory of Crystal Lattices* (Oxford U. P., New York, 1956).
[18]R. A. Cowley, Phys. Rev. 134, A981 (1964).

PHYSICAL REVIEW B VOLUME 5, NUMBER 5 1 MARCH 1972

Interacting Magnons in the Linear Chain*

Hans C. Fogedby†
Department of Physics, Harvard University, Cambridge, Massachusetts 02138
(Received 8 June 1971)

The magnon bound-state spectrum recently observed in the anisotropic magnetic salt $CoCl_2 \cdot 2H_2O$ is investigated by means of response functions. A perturbation scheme is set up for the response functions and the transverse and longitudinal susceptibilities are evaluated to second order in the transverse anisotropy. The effects of the Heisenberg part of the exchange interaction are included to second order by solving a two-magnon and a three-magnon scattering problem. In the zero-field limit we evaluate under certain simplifying assumptions the transverse susceptibility to all orders in the transverse anisotropy.

I. INTRODUCTION

The recent observations by Torrance and Tinkham[1,2] of a magnon bound-state spectrum in the magnetic crystal $CoCl_2 \cdot 2H_2O$ have stimulated renewed theoretical interest in the dynamical properties of the linear anisotropic magnetic chain. The authors[1-3] showed that their helium temperature measurements of the absorption spectra could be interpreted in terms of the spin-$\frac{1}{2}$ Hamiltonian

$$H = -2\sum_{i=1}^{N}\left[-\tfrac{1}{2}g^{z}\mu_B H_0 S_i^{z} + j^{z} S_i^{z} S_{i+1}^{z} + \tfrac{1}{2} j^{\perp}(S_i^{+}S_{i+1}^{-} + \text{H. c.}) + \tfrac{1}{2} j^{a}(S_i^{+}S_{i+1}^{+} + \text{H. c.})\right], \quad (1.1)$$

which describes a single cluster of exchange-coupled Co^{++} ions. We have included a Zeeman term arising from an applied magnetic field in the z direction. The spin operators satisfy the usual commutation relations

$$[S_i^{\pm}, S_k^{z}] = \mp S_i^{\pm}\delta_{ik} \quad (1.2)$$

and

$$[S_i^{-}, S_k^{+}] = -2S_i^{z}\delta_{ik}, \quad (1.3)$$

where we have chosen units such that $\hbar = 1$. Furthermore, in the spin-$\frac{1}{2}$ case we obtain the length condition

$$S_i^{+}S_i^{-} - S_i^{z} = \tfrac{1}{2} \quad (1.4)$$

and the minimum equations

$$S_i^{+}S_i^{+} = S_i^{-}S_i^{-} = 0 \quad \text{and} \quad S_i^{z}S_i^{z} = \tfrac{1}{4}. \quad (1.5)$$

The longitudinal and transverse anisotropy of the exchange Hamiltonian (1.1) is characterized by the nearest-neighbor exchange constants j^{z}, $j^{\perp}$, and j^{a} [where $j^{\perp} = \frac{1}{2}(j^{x} + j^{y})$ and $j^{a} = \frac{1}{2}(j^{x} - j^{y})$], and by the spectroscopic splitting factors g^{z}, g^{x}, and g^{y}. The dimensionless anisotropy parameters $\sigma = j^{\perp}/j^{z}$ and $\alpha = j^{a}/j^{z}$ assume the values 0.2 and 0.08, respectively, in the case of $CoCl_2 \cdot 2H_2O$.

Owing to the strong longitudinal anisotropy and to the fact that j^{z} is of order 17 °K for $CoCl_2 \cdot 2H_2O$ the measurements by Torrance and Tinkham probe only the zero temperature properties of the system. Any temperature dependence of the excitation spectrum will be exponentially small, i.e., of order $e^{-17/T}$. Consequently, we shall in the present paper confine our attention to zero temperature.

The strong longitudinal anisotropy of the exchange Hamiltonian (1.1) suggests treating the linear chain as a one-dimensional Ising model in the lowest approximation. Such an approach was in fact carried out by Torrance and Tinkham,[1,3] who constructed Bloch functions for the localized Ising spin deviations and computed numerically the effects on the